

Lattice Boltzmann interface capturing method for incompressible flows

H. W. Zheng, C. Shu,* and Y. T. Chew

Department of Mechanical Engineering, National University of Singapore, 119260 Singapore

(Received 14 April 2005; revised manuscript received 22 July 2005; published 11 November 2005)

A lattice Boltzmann interface capturing method for incompressible flows is proposed in this paper. The interface is naturally captured by minimizing the free energy functional. It is easily implemented and does not require interface reconstruction as required by most of the traditional interface tracking methods such as the volume of fluid method. Moreover, the method does not require the isotropic property of the fourth order lattice tensor as do other lattice Boltzmann methods. Thus the D2Q5 (D2 means two dimensional, Q5 means five velocity model) discrete velocity model is applied in the method. The interface profile along the flat interface and coexistence curve can be given analytically. The proposed method is validated for some test cases, and compared to the volume of fluid and level set methods. Numerical results show that the present method performs very well and can generate very sharp interfaces.

DOI: [10.1103/PhysRevE.72.056705](https://doi.org/10.1103/PhysRevE.72.056705)

PACS number(s): 47.11.+j, 45.50.-j

I. INTRODUCTION

Lattice Boltzmann method has received much attention since the 1980s due to its simplicity and easy implementation. It has been proven to be a useful tool for solving complex flows and flows in complex geometries, such as multiphase [1–4], free surface [5], porous media flow with moving boundaries and suspension [6] *etc.* An efficient scheme to predict the interface accurately is essential for those problems. In fact, the interface tracking or capturing is a challenging and critical issue for multiphase flows.

To track or capture the interface, the popular methods in traditional computational fluid dynamics (CFD) are the Volume of Fluid (VOF) [7–11] and the level set method [12]. Both of them solve a scalar transport equation in the Eulerian frame. In fact, the VOF method does not track the interface itself. Instead, it tracks the volume fraction of each phase and component [11]. The interface is reconstructed from the values of volume fraction. In this sense, it is often called the volume tracking method. This shows that the VOF approach cannot easily be extended to three dimensional applications. Besides, as stated by Pilliod *et al.* [11], most of VOF interface reconstruction schemes only have the first order accuracy. In contrast, the level set method utilizes a level set function to indicate the interface. One advantage is that the level set function varies smoothly across the interface while the volume fraction is discontinuous. However, the level set method requires a re-initialization procedure to keep the distance property when large topological changes occur around the interface. This may violate mass conservation for each phase or component [13].

In the lattice Boltzmann method, three main models have been developed for multiphase and multicomponent flows during the past twenty years. They are color method [14,15], potential method [16], and free energy method [1–3,17]. The color and potential methods do not track the interface explicitly. In these two methods, the interface is considered as the

region where the gradient of density difference is not zero. The free energy method naturally captures the interface by explicitly solving a convection-diffusion equation. A distribution function is designed to solve this equation. Based on the Chapman Enskog expansion, it can be shown that the distribution function will recover the modified Cahn-Hilliard equation [18] which is an evolution equation for the interface. This equation evolves the order parameter (for example, density difference) which is used to distinguish the different phases or components. In this sense, the order parameter is quite similar to the indicator of the traditional tracking methods such as VOF and level set method. However, the original free energy method does not completely recover the convective Cahn-Hilliard equation but with two additional terms. Another limitation is that the density difference of each phase or component must not be too large. To remove this limitation, Inamuro *et al.* [4] proposed a model based on the free energy method to simulate multiphase flows with a large density ratio. In their method, the interface capturing is decoupled from the fluid flow solver. It is quite similar to the traditional treatment of VOF method [19] and level set method [20], in which the pressure correction is applied to enforce the continuity condition after every collision-stream step. On the other hand, their method also shows some deficiency. The physics of the interface evolution equation is not clear. Besides, as can be seen from the Results and Discussion part of this paper, it will generate some unphysical disturbances in some cases such as shear flow even though the local divergence of velocity field is zero. In this sense, it may not be correct for some incompressible flows although the projection procedure is employed to secure the incompressibility condition. Furthermore, the minima and maxima of the order parameter are not given analytically. Thus it is not easy to define a reasonable cutoff value. To remove these difficulties, a new method is proposed in this paper. In our method, we solve the convective Cahn-Hilliard equation instead of scalar transport equation. It overcomes the deficiencies of Inamuro *et al.*'s method in three aspects. First, it removes the additional terms by applying a modified lattice Boltzmann method. The additional terms also appeared in the work of Swift *et al.* [17].

*Corresponding author. Email address: mpeshuc@nus.edu.sg

Second, it replaces the pressure tensor with chemical potential. Third, it uses another free energy functional which has a good property such that the interface profile and coexistence curve can be given analytically.

The paper is organized as follows. Section II outlines the new interface capturing method. It recovers the convective Cahn Hilliard equation to the second order without the additional terms appeared in the work of Swift *et al.* [17]. The proposed method will then be verified and applied to some test cases in Sec. III. The numerical results will be compared with those from other methods such as VOF and level set method. Finally, the conclusion will be drawn in Sec. IV.

II. METHODOLOGY

A. The interface capturing equation

The interface capturing is modeled by an evolution equation of the order parameter ϕ , which serves as a counterpart of the volume fraction in VOF method and level set function in the level set method,

$$\frac{\partial \phi}{\partial t} + \nabla \cdot (\phi u) = \theta_M \nabla^2 \mu_\phi, \quad (1)$$

where θ_M is called mobility and μ_ϕ is the chemical potential. Equation (1) is a convective Cahn-Hilliard equation [18]. The chemical potential is approximately a constant when the system approaches an equilibrium state. Thus Eq. (1) is similar to the interface transport equation of VOF or level set method where the corresponding right-hand side is zero.

This equation has been investigated by many researchers [2,17]. However, they did not completely recover to the convective Cahn-Hilliard equation. For example, as shown in Swift *et al.* [17], it recovers the equation below with the second order accuracy

$$\begin{aligned} \partial_t \phi + \nabla \cdot (\phi u) - \left(\tau - \frac{1}{2} \right) \delta(\nabla^2(\Gamma \mu) + \nabla \nabla : (\phi u u)) \\ + \partial_t \nabla \cdot (\phi u) + O(\delta^2) = 0. \end{aligned} \quad (2)$$

Inamuro *et al.* [4] proposed a similar method to capture the interface. They used another equation

$$\frac{\partial \phi}{\partial t} + \nabla \cdot (\phi u) = \nabla \cdot (\nabla \cdot P), \quad (3)$$

where P is the pressure tensor. This equation is quite similar to Eq. (1). But its physical background is not very clear.

The chemical potential is related to the free energy density functional. To distinguish different phases, we choose the free energy functional [21] as

$$F = \int \text{Im}(\phi, \nabla \phi) dV = \int dV \left\{ \psi(\phi) + \frac{\kappa}{2} (\nabla \phi)^2 \right\}, \quad (4)$$

where κ is related to the surface energy, and the bulk free energy density

$$\psi(\phi) = a(\phi^2 - \phi^{*2})^2, \quad (5)$$

where ϕ^* is a constant which is related to the equilibrium state. Equation (4) ensures smooth local deviations near the

interface. The energy density (5) will give two stable states (where the bulk free energy density is zero) of the system. We can also obtain the coexistence curve as

$$\phi = \pm \phi^*. \quad (6)$$

Thus the positions, where the condition $\phi=0$ is satisfied, are defining the interface; while the regions where $\phi < 0$ and $\phi > 0$ represent the two phases or components, respectively.

The equilibrium conditions are obtained by minimizing the free energy functional F subject to a constant constraint (the total order parameter is conserved in the whole field)

$$\Phi = \int \phi dV. \quad (7)$$

The above process leads to minimizing the functional

$$E(\phi) = \int \text{Im}(\phi, \nabla \phi) dV + \mu_\phi (\Phi - \int \phi dV). \quad (8)$$

To obtain a differential equation for the equilibrium, we minimize E and obtain

$$\frac{\partial \text{Im}}{\partial \phi} - \nabla \cdot \frac{\partial \text{Im}}{\partial \nabla \phi} - \mu_\phi = 0. \quad (9)$$

This is the Euler-Lagrange equation. Thus we can easily derive the chemical potential as

$$\mu_\phi = \frac{\partial \text{Im}}{\partial \phi} - \nabla \cdot \frac{\partial \text{Im}}{\partial \nabla \phi} = a(4\phi^3 - 4\phi^{*2}\phi) - \kappa \nabla^2 \phi. \quad (10)$$

B. The implementation of lattice Boltzmann method

Under the lattice Boltzmann framework, Eq. (1) can be solved by iterating the evolution equation for a set of distribution functions. Thus we do not need to solve the continuous convection-diffusion equation (1) but the lattice Boltzmann equation. The chemical potential will be included in the lattice Boltzmann equation through the equilibrium distribution function $f_i^{(0)}$.

This distribution function evolves with a modified lattice Boltzmann equation [22] and BGK approximation [23],

$$f_i(x + e_i \delta, t + \delta) = f_i(x, t) + (1 - q)[f_i(x + e_i \delta, t) - f_i(x, t)] + \Omega_i, \quad (11)$$

with

$$\Omega_i = \frac{f_i^{(0)}(x, t) - f_i(x, t)}{\tau_\phi}, \quad (12)$$

where f_i is the distribution function, Ω_i is the collision term, τ_ϕ is the dimensionless single relaxation time, e_i is the lattice velocity, and q is a constant coefficient. It will reduce to the conventional lattice Boltzmann equation when q is set to be one.

The macroscopic variable (order parameter) ϕ is evaluated by

$$\phi = \sum_i f_i. \quad (13)$$

By using the Taylor series expansion to the second order, Eq. (11) can be rewritten as

$$\begin{aligned} & \delta(\partial_t + e_i \cdot \nabla) f_i + \frac{1}{2} \delta^2 (\partial_t + e_i \cdot \nabla)^2 f_i \\ & + (q-1) \left[\delta(e_i \cdot \nabla) f_i + \frac{1}{2} \delta^2 (e_i \cdot \nabla)^2 f_i \right] + O(\delta^3) = \Omega_i. \end{aligned} \quad (14)$$

Furthermore, by applying the Chapman-Enskog expansion to Eq. (14),

$$\begin{aligned} f_i & \approx f_i^{(0)} + \varepsilon f_i^{(1)} + \varepsilon^2 f_i^{(2)}, \\ \partial_t & \approx \varepsilon \partial_{t0} + \varepsilon^2 \partial_{t1}, \\ \partial_x & \approx \varepsilon \partial_{x1}, \\ \Omega & \approx \Omega^{(0)} + \varepsilon \Omega^{(1)} + \varepsilon^2 \Omega^{(2)}, \end{aligned} \quad (15)$$

we can show (see the Appendix) that if the distribution function satisfies the conservation laws

$$\sum_i f_i^{(0)} = \phi, \quad (16)$$

$$\sum_i f_i^{(0)} e_{i\alpha} \equiv \frac{1}{q} \phi u_\alpha, \quad (17)$$

$$\sum_i f_i^{(0)} e_{i\alpha} e_{i\beta} = \Gamma \mu_\phi \delta_{\alpha\beta}, \quad (18)$$

and the coefficient q is set to be

$$q = \frac{1}{\tau_\phi + 0.5}, \quad (19)$$

then Eq. (11) recovers the Cahn Hilliard equation with the second order of accuracy

$$\partial_t \phi + \nabla \cdot (\phi u) - \theta_M \nabla^2 \mu_\phi + O(\delta^2) = 0, \quad (20)$$

where the mobility is defined as

$$\theta_M = q \left(\tau_\phi q - \frac{1}{2} \right) \delta \Gamma. \quad (21)$$

Equation (17) is not used to evaluate the velocity. In fact, the velocity field is given in advance in most of interface tracking methods which also used in our method. Equation (18) is different from the other free energy-based lattice Boltzmann methods [17]. For example, Swift *et al.* [17] used

$$\sum_i f_i^{(0)} e_{i\alpha} e_{i\beta} = \Gamma \mu_\phi \delta_{\alpha\beta} + \phi u_\alpha u_\beta.$$

Besides, Eq. (18) also shows that it does not require the fourth order isotropic lattice tensor as the conventional lattice Boltzmann methods need. Thus, D2Q5 (D2 means two

dimensional, Q5 means five velocity model) model is used in the paper. That is, the discrete velocities are

$$e_1 = (0 \ 0)^T, \quad e_{2,4} = (\pm 1 \ 0)^T, \quad e_{3,5} = (0 \ \pm 1)^T. \quad (22)$$

To recover Eq. (1), according to Eqs. (16)–(18), the equilibrium distribution function in Eq. (11) is expanded only to the first order of velocity as follows:

$$f_i^{(0)} = A_i + B_i \phi + C_i \phi e_i \cdot u. \quad (23)$$

The coefficients are taken as

$$B_1 = 1, B_2 = \dots = B_5 = 0,$$

$$C_i = \frac{1}{2q} \quad (i = 1, \dots, 5),$$

$$A_i = D_i \Gamma \mu_\phi \quad (i = 1, \dots, 5),$$

$$D_1 = -2, D_i = \frac{1}{2} \quad (i = 2, \dots, 5), \quad (24)$$

where Γ is used to control the mobility. In the LBM implementation, the second order derivative in Eq. (10) is evaluated by

$$\nabla^2 \phi = \frac{1}{(\delta t)^2} \sum_i [\phi(x + e_i \delta t) - \phi(x)]. \quad (25)$$

III. RESULTS AND DISCUSSION

A. Verification

In the state of equilibrium, the interface profile satisfies

$$\mu_\phi = 0. \quad (26)$$

For the flat interface, we can integrate this equation to obtain the profile. Following the same procedure as Jacqmin *et al.* [24], we can obtain from Eqs. (5), (10), and (26) as

$$\frac{\kappa}{2} \left(\frac{d\phi}{d\zeta} \right)^2 = a(\phi - \phi^*)^2 (\phi + \phi^*)^2, \quad (27)$$

where ζ is the coordinate which is perpendicular to the interface. The original point is at the interface.

By integrating the above equation (27) and using the following relationship,

$$\frac{d \tanh \zeta}{d\zeta} = 1 - (\tanh \zeta)^2,$$

we can obtain the profile along the normal direction of the interface as

$$\phi = \phi^* \tanh(\pm 2\zeta/W), \quad (28)$$

where the interface thickness is

$$W = \frac{\sqrt{2\kappa/a}}{\phi^*}. \quad (29)$$

Equation (28) is used to verify the present method. The sign in the bracket is dependent on the initial condition of the problem.

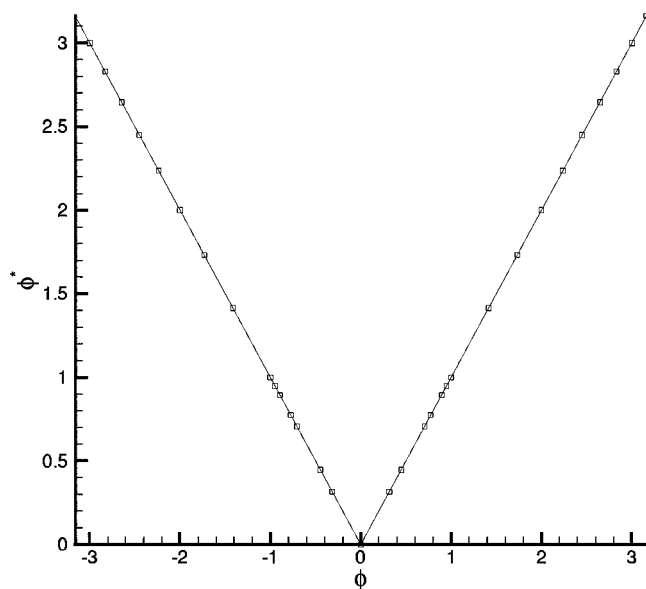


FIG. 1. Coexistence curve.

Initially, a circular disk is located at the center of domain. The mesh size used is 200×200 . Periodic boundary conditions are employed at all boundaries. The parameters κ , Γ , a , and τ_ϕ are fixed as $\kappa=0.002$, $\Gamma=0.4$, $a=0.001$, and $\tau_\phi=0.7$. Only the parameter ϕ^* is tuned for the simulation. Initially, the order parameter is set to be $-0.9\phi^*$ inside the disk and $0.9\phi^*$ elsewhere. For this problem, the analytical interface profile can be expressed as

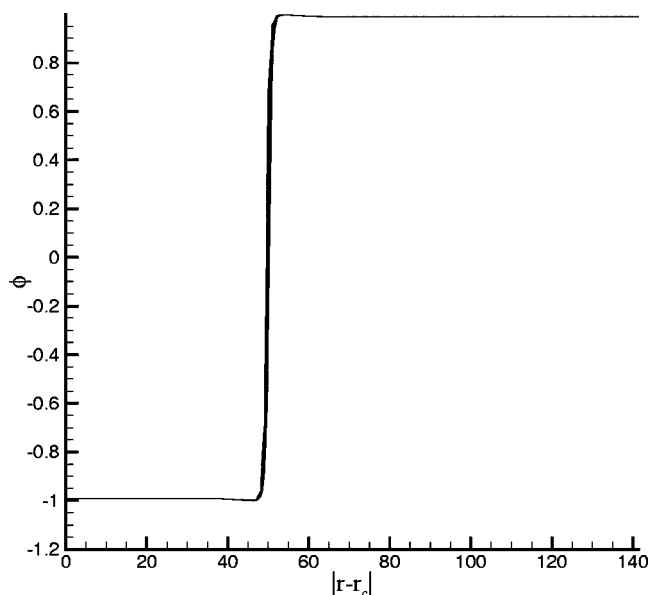
$$\begin{aligned} \phi &= \phi^* \tanh[2(r_c - R)/W] \\ &= \phi^* \tanh[2(\sqrt{(x - x_c)^2 + (y - y_c)^2} - R)/W], \end{aligned} \quad (30)$$

where r_c is the distance between the point (x, y) and the center of the disk and R is the radius of the disk.

We observe the minimum and maximum values of the order parameter. From the coexistence curve as shown in Fig. 1, it is easily found that the observed values are in agreement with the theoretical prediction derived by minimizing the bulk free energy. Figure 2 displays the order parameter at all lattice points as a function of the distance from the center point which shows clearly that it is independent on the direction. Thus, it shows that the disk is isotropic. In fact, this curve is the profile described by Eq. (30). To see this clearly, we redraw the order parameter along the central axis parallel to the x direction. As illustrated in Fig. 3, the numerical order parameter profile (denoted as rectangle) agrees with the analytic solution (the solid line) very well.

B. Simple translation

The simple translation is a basic test case for many interface capturing or tracking methods. A hollow square is put near the left top corner as shown in Fig. 4(a). The mesh size used is 200×200 , that is, $i, j \in [0, 200]$. The center of the hollow square is $(40, 160)$. The width (or height) of the exterior and interior squares is 60 and 20 in lattice unit, respectively. The periodic boundary condition is employed at all


 FIG. 2. Verification of isotropy for $\phi^*=1$.

boundaries. The parameters are chosen as $\kappa=0.002$, $\Gamma=0.4$, $\phi^*=1$, $\tau_\phi=0.7$, and $a=0.001$. Initially, the order parameter is set to be ϕ^* inside the square and $-\phi^*$ elsewhere.

The unidirectional velocity is

$$u = 2u_0, \quad v = -u_0, \quad (31)$$

with

$$u_0 = 0.01.$$

This velocity is chosen not to align with the coordinate axis and the lattice direction in order to show the independence of these two directions. Because of the intrinsic low Mach number limit of the LB method, the magnitude of the velocity

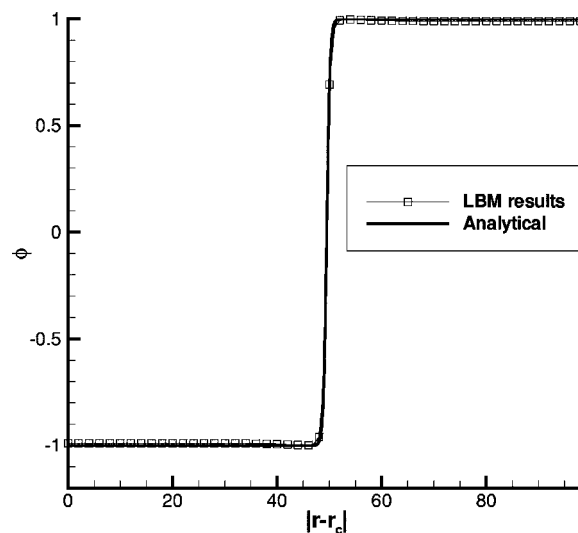


FIG. 3. Order parameter profile along the normal direction of the interface as a function of the distance from the center of the disk (LBM result is drawn every two points).

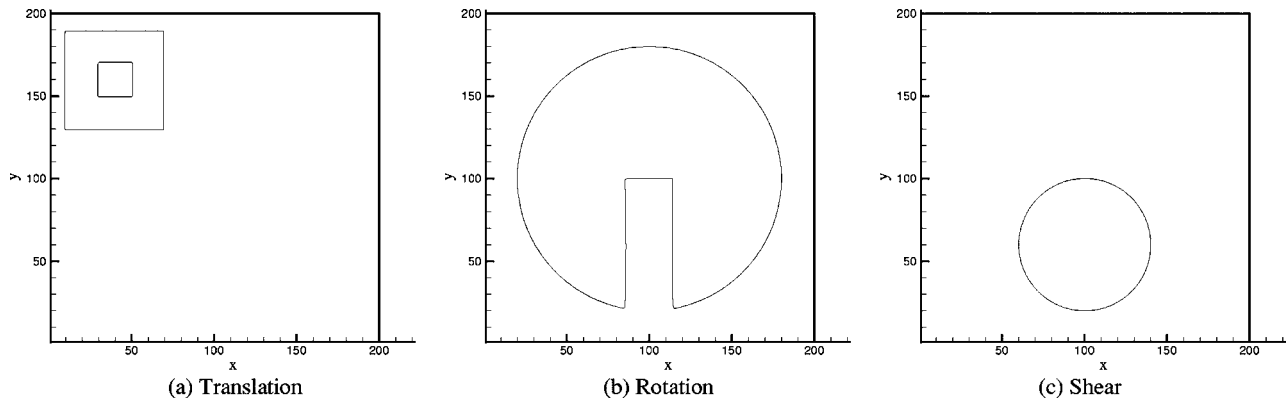


FIG. 4. Initial conditions.

must not be too large. Thus the scale parameter u_0 is used in the present study.

When the physical velocity (the unit is meter/second) is taken as

$$u^{phys} = 2, \quad v^{phys} = -1, \quad (32)$$

and physical domain (the unit is meter) is

$$x^{phys}, y^{phys} \in [0, 2],$$

then the physical time t^{phy} and the scaled time t has the following relationship:

$$t^{phys} = 10^{-4}t. \quad (33)$$

To validate our method, we compare our results with those of Hirt-Nichol's VOF [7] and level set method [12]. The initial velocity is set to be the value given by Eq. (31). We plot the interface figure at 0.6 seconds (physical time) for the three methods. For this case, there is an analytical solution for the interface position. As we can expect, the center of the square should be (160,100) at this moment. In these contour plots (and all others below), the contour level of the Hirt-Nichol's method, level set method, and present method are 0.5, 0, and 0, respectively for the interface. From Fig. 5, we can see clearly that the VOF results are jagged in the vicinity of the interface. Besides, the shape is substantially twisted at the square corner. This suggests that Hirt-Nichol's VOF gives a poor interface tracking. The results of level set method and present approach are much better than Hirt-Nichol's VOF

results. For this case, the level set method shows a slightly better performance than our approach.

C. Solid body rotation

Zalesak's disk is widely used as a test case to validate the interface tracking method. The surface of Zalesak's disk is a combination of a curve with a slot as illustrated in Fig. 4(b). That is, it consists of curve and several straight lines. The objective of this section is to test whether the curve and line will keep their shapes under a rotational velocity field as shown below. Like the previous example, the computational domain is a square with $0 \leq i, j \leq 200$. The radius of the disk is 80 and the width of the slot is 15 in lattice unit. The periodic boundary condition is employed at all boundaries. The parameters are chosen as those in Sec. III B. Initially, the disk is located at the center of the square; the order parameter is set to be ϕ^* inside the disk and $-\phi^*$ elsewhere. The rotational velocity is given by the stream function

$$\Psi = u_0 \pi [(x - 0.5)^2 + (y - 0.5)^2], \quad (34)$$

where u_0 is the scaled parameter and is taken as 0.02, NX is the number of mesh points in the x direction. Thus, the velocity is computed by

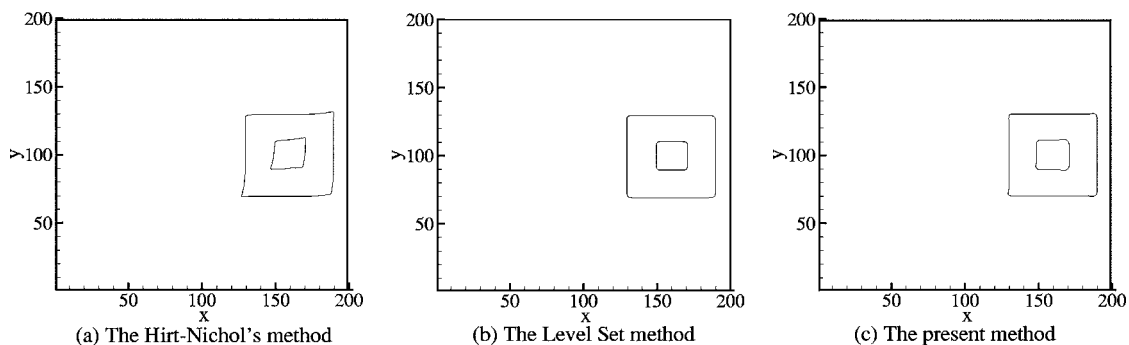


FIG. 5. Results of simple translation by different methods.

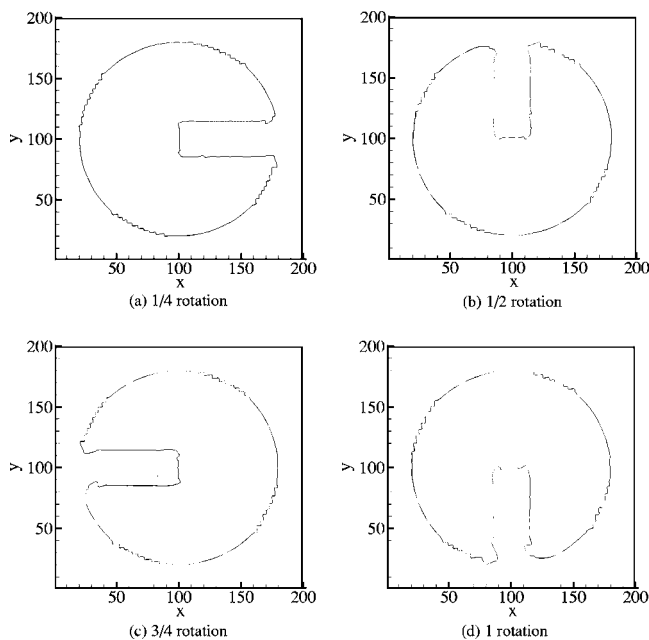


FIG. 6. Results of the Hirt-Nicol's VOF method.

$$u = -u_0\pi\left(\frac{j}{NY} - 0.5\right), \quad v = u_0\pi\left(\frac{i}{NX} - 0.5\right), \quad u_0 = 0.02. \quad (35)$$

Obviously, there is no preferred direction in the velocity. Like the previous example, the scaled parameter u_0 is used in the present computation.

When the physical velocity field (the unit is meter/second) is taken as

$$u^{phys} = -\pi(y^{phys} - 0.5), \quad v^{phys} = \pi(x^{phys} - 0.5), \quad (36)$$

and physical domain (the unit is meter) is chosen as

$$x^{phys}, y^{phys} \in [0, 1],$$

we can get the relationship between the physical time t^{phy} and the scaled time t ($NX=NY$) as

$$t^{phys} = \frac{1/NX}{1/u_0} t = \frac{u_0}{NX} t. \quad (37)$$

With $u_0=0.02$ and $NX=200$, it is clear that 10 000 time steps in the present computation corresponds to one second in other methods. To evaluate our method, we also compare our results with those of Hirt-Nicol's VOF and level set method. For this case, there is also an analytical solution for the interface position. The disk should keep its shape as the initial state after one rotation. From Fig. 6, we can observe that Hirt-Nicol's results are jagged around the interface. Besides, the shape is substantially twisted near corner regions. This indicates that Hirt-Nicol's VOF gives a poor interface tracking. In contrast, Figs. 7 and 8 show that both the level set and the present methods generate accurate results except that the sharp corners at ends of the slot become rounded. Furthermore, we can see from Fig. 7 that there is some diffusion around the tip generated by the level set method (re-

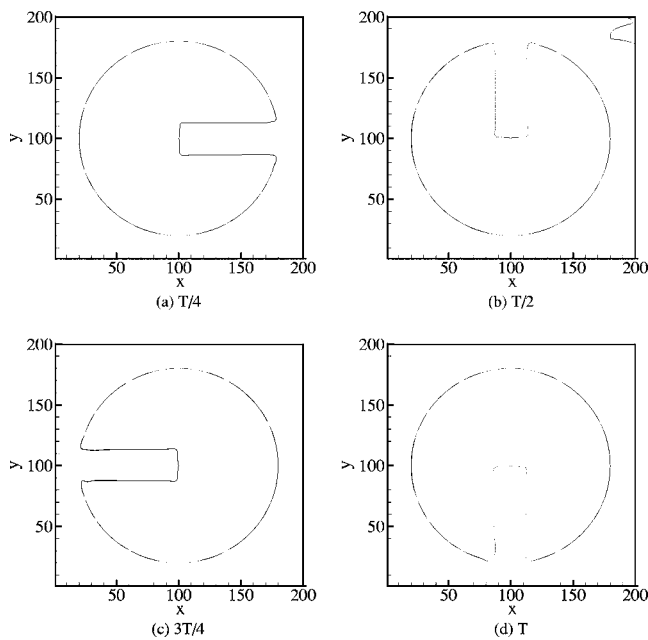


FIG. 7. Results of the level set method.

sult of 1/2 rotation). As shown in Fig. 8, this numerical diffusion is not found in the present method. In this sense, we can say that the present method performs better than the level set method for this test case.

D. Shear flow

As shown in Secs. III B and III C, the simple translation and solid body rotation tests do not induce large topological changes. As pointed out by Rudman [25], the velocity field of these cases is very special. It not only satisfies the continuity equation but also $\partial u/\partial x=0$ and $\partial v/\partial y=0$. This contrib-

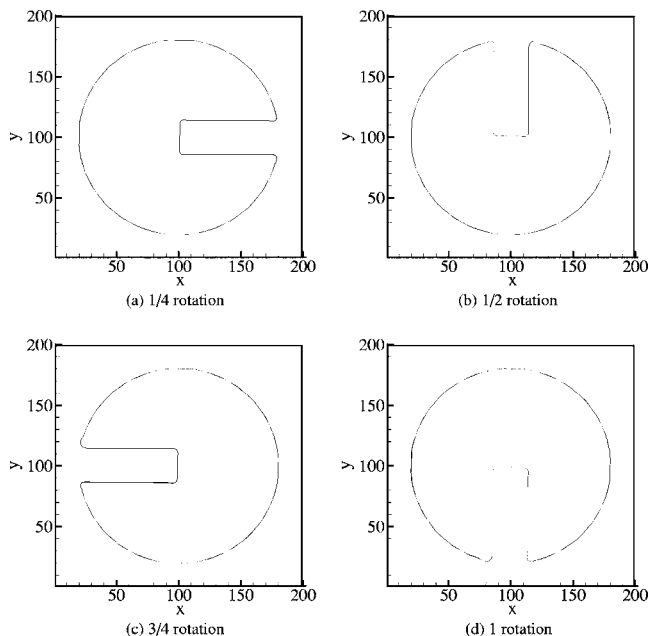


FIG. 8. Results of the present method.

utes to the results where the shape does not deform during the whole process. The two cases well verify the Galilean invariance of the method.

In this section, we will consider a more realistic case, that is, rotation of a disk under shear flow. Again, the computational domain is taken as a square with $0 \leq i, j \leq 200$. The radius of the disk is 40, while the center of the disk is (100, 60). Periodic boundary conditions are employed at all boundaries. The parameters are also chosen as those in Sec. III B. Initially, the disk is located at the bottom part of the square as shown in Fig. 4(c), and the order parameter is set to be ϕ^* inside the disk and $-\phi^*$ elsewhere.

During the process before one rotation cycle T , the stream function is taken as

$$\Psi = u_0 \cos[\pi(x - 0.5)] \cos[\pi(y - 0.5)]. \quad (38)$$

Thus the shear velocity is computed as

$$\begin{aligned} u &= u_0 \pi \cos \left[\pi \left(\frac{i}{NX} - 0.5 \right) \right] \sin \left[\pi \left(\frac{j}{NY} - 0.5 \right) \right], \\ v &= -u_0 \pi \sin \left[\pi \left(\frac{i}{NX} - 0.5 \right) \right] \cos \left[\pi \left(\frac{j}{NY} - 0.5 \right) \right], \\ u_0 &= 0.01. \end{aligned} \quad (39)$$

When the physical velocity field (the unit is meter/second) is taken as

$$\begin{aligned} u^{phys} &= -\pi \cos[\pi(x^{phys} - 0.5)] \sin[\pi(y^{phys} - 0.5)], \\ v^{phys} &= \pi \sin[\pi(x^{phys} - 0.5)] \cos[\pi(y^{phys} - 0.5)], \end{aligned} \quad (40)$$

and physical domain (the unit is meter) is

$$x^{phys}, y^{phys} \in [0, 1],$$

we can get the relationship between physical time t^{phy} and the scaled time t ($NX=NY$) as

$$t^{phys} = \frac{1/NX}{1/u_0} t = \frac{u_0}{NX} t. \quad (41)$$

In the present computation, $u_0=0.01$ and $NX=NY=200$. Thus 5000 time steps correspond to one second in other methods.

After one rotation cycle, we adjust the rotation direction by changing the sign of the velocity field and continue to run the code for another cycle T . We try to see whether the shape of disk would return to its initial configuration. The present results are illustrated in Fig. 12. Obviously, the disk returns to its original position with a little distortion.

To further show the performance of present method, the same problem was solved by other methods. First, we apply the method of Inamuro *et al.* [4]. The equilibrium distribution function of the method proposed by Inamuro *et al.* is

$$\begin{aligned} f_i^{(0)} &= d_i \left(p_0 - \kappa \phi \nabla^2 \phi - \frac{\kappa}{6} |\nabla \phi|^2 \right) + b_i \phi + 3w_i \phi e_i \cdot u \\ &\quad + w_i \kappa G_{\alpha\beta} e_{i\alpha} e_{i\beta}, \end{aligned} \quad (42)$$

where

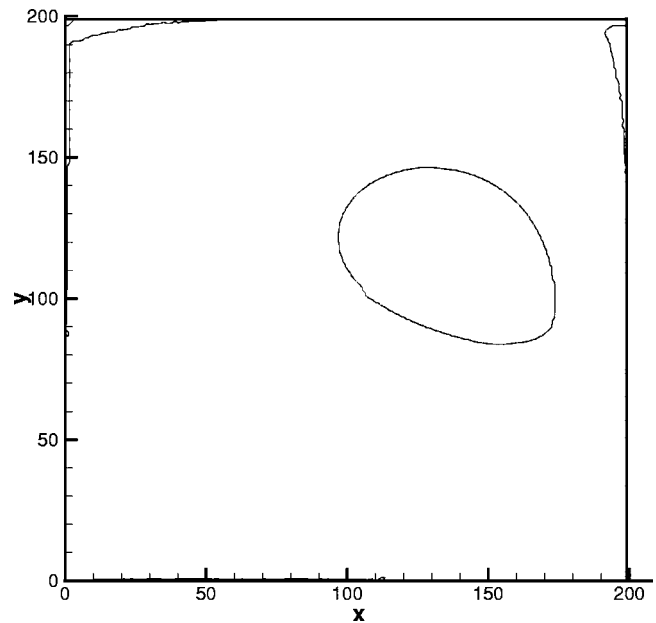


FIG. 9. Some disturbances generated by the method of Inamuro *et al.* [4].

$$p_0 = \frac{\phi T}{1 - d\phi} - b\phi^2,$$

$$b_1 = 1, \quad b_2 = \dots = b_9 = 0,$$

$$w_1 = \frac{4}{9}, \quad w_2 = \dots = w_5 = \frac{1}{9}, \quad w_6 = \dots = w_9 = \frac{1}{36},$$

$$a_i = d_i \Gamma \mu_\phi (i = 1, \dots, 9),$$

$$d_1 = -\frac{5}{3}, \quad d_i = 3w_i (i = 2, \dots, 9). \quad (43)$$

Note that the original paper is for 3D simulation. We re-write its correspondent 2D equilibrium function as shown above. In the simulation, b , d , and T in Eq. (43) are chosen as 1, 1, and 0.293, respectively. The result of Inamuro *et al.*'s method is shown in Fig. 9, which is obtained after a few hundred time steps. We need to point out that Inamuro *et al.*'s method also performs well in the Zalesak's disk case. However, we can see clearly that some unphysical disturbances appear at the corner for this case even though the computation only marches a few hundred time steps. If we continue to do the simulation, the disturbances will expand until the disk and the disturbances coalesce together eventually. Hirt-Nichol's VOF, level set method are also applied to solve this problem. Their results are displayed respectively in Figs. 10 and 11. From Fig. 10, it is obvious that the Hirt-Nichol's VOF shows quantities of jetsam and sawteeth at the interface as mentioned by many investigators. As shown in Figs. 11 and 12, both the level set method and the present method generate a relatively sharp solution although they did not completely recover the initial configuration. This implies

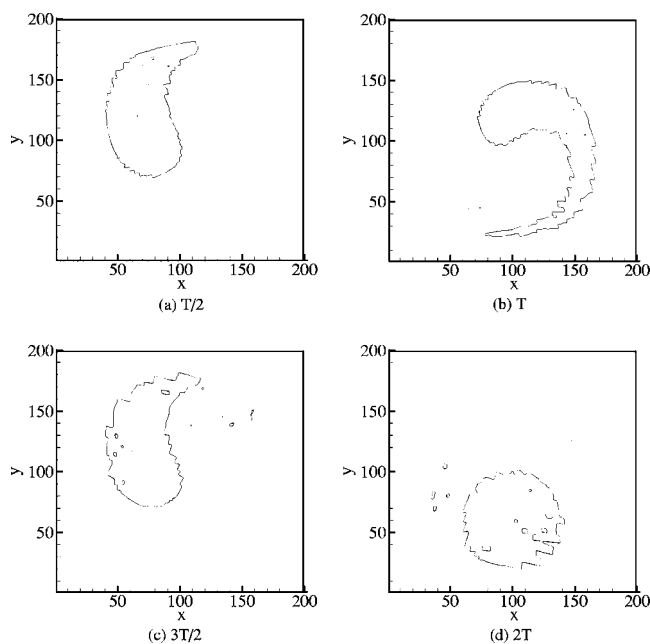


FIG. 10. Results of the Hirt-Nicol's VOF method.

that the present method and the level set method perform very well for this test case.

IV. CONCLUSIONS

A lattice Boltzmann interface tracking method is developed in this paper. It does not require interface reconstruction as needed by most of the traditional methods. The order parameter and interface evolution equation (Cahn-Hilliard equation) have a physical background which is derived from the free energy functional. They are different from volume fraction or level set function and the transport equation,

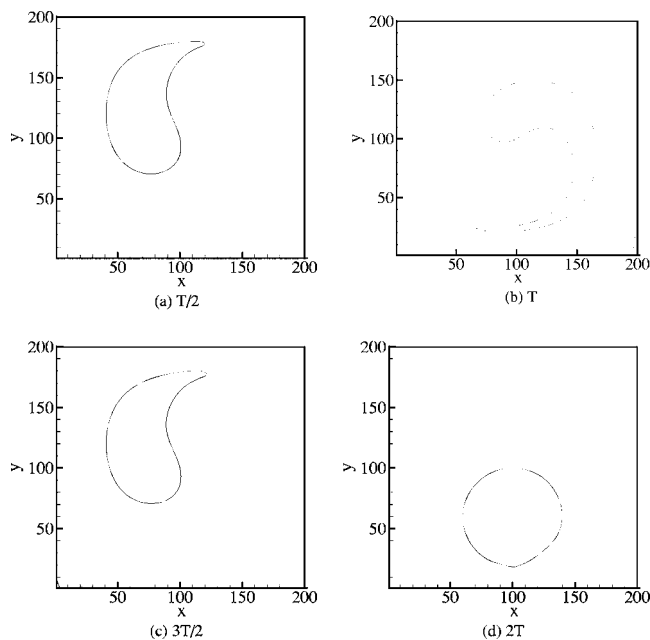


FIG. 11. Result of the level set method.

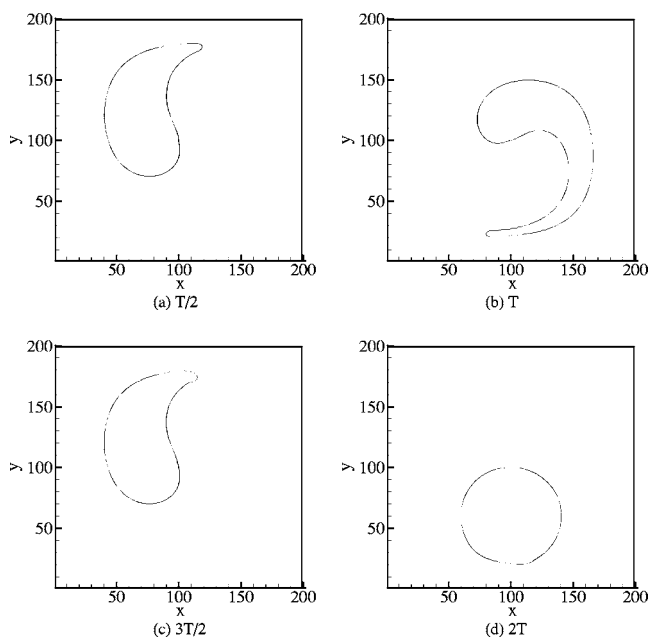


FIG. 12. Result of the present method.

which is used in the volume of fluid and level set methods. The five discrete velocity model (D2Q5) can be used. It seems that the present method has a better efficiency than the method of Inamuro *et al.* [4] since it only evaluates the second order derivatives while the latter needs to evaluate both the first order and the second order derivatives. However, our method costs more CPU time than the level set method and the VOF method. Numerical results show that the present method can capture accurate position of the interface and keep its sharpness. For example, it generates relatively sharp interfaces and shows good performance under shear flow with stretching and tearing. Furthermore, our method can be easily extended to the three-dimensional case with D3Q7 model. Thus the efficiency is quite good for three-dimensional applications. For this part, we will prepare another paper.

APPENDIX

The modified lattice Boltzmann equation can be written as

$$f_i(x + e_i \delta, t + \delta) = f_i(x, t) + (1 - q)[f_i(x + e_i \delta, t) - f_i(x, t)] + \Omega_i, \tag{A1}$$

where

$$\Omega_i = \frac{f_i^{(0)}(x, t) - f_i(x, t)}{\tau}. \tag{A2}$$

By using the Taylor series expansion to the second order, Eq. (A1) can be rewritten as

$$\begin{aligned} & \delta(\partial_t + e_i \cdot \nabla) f_i + \frac{1}{2} \delta^2 (\partial_t + e_i \cdot \nabla)^2 f_i \\ & + (q-1) \left[\delta(e_i \cdot \nabla) f_i + \frac{1}{2} \delta^2 (e_i \cdot \nabla)^2 f_i \right] + O(\delta^4) = \Omega_i. \end{aligned} \quad (\text{A3})$$

By applying the Chapman-Enskog expansion to Eq. (A3),

$$f_i \approx f_i^{(0)} + \varepsilon f_i^{(1)} + \varepsilon^2 f_i^{(2)}, \quad (\text{A4})$$

$$\partial_t \approx \sum_k \varepsilon^{k+1} \partial_{t^k} = \varepsilon \partial_{t^0} + \varepsilon^2 \partial_{t^1}, \quad (\text{A5})$$

$$\partial_x \approx \varepsilon \partial_{x^1}, \quad (\text{A6})$$

$$\Omega \approx \Omega^{(0)} + \varepsilon \Omega^{(1)} + \varepsilon^2 \Omega^{(2)}, \quad (\text{A7})$$

we then have

$$\varepsilon [\delta(\partial_{t^0} + q e_i \cdot \nabla_1) f_i^{(0)}] = -\frac{\varepsilon}{\tau} f_i^{(1)}, \quad (\text{A8})$$

in the order of $O(\varepsilon)$, and

$$\begin{aligned} & \varepsilon^2 \left[\delta \partial_{t^1} f_i^{(0)} + \delta(\partial_{t^0} + e_i \cdot \nabla_1) f_i^{(1)} + \frac{1}{2} \delta^2 (\partial_{t^0} + e_i \cdot \nabla_1)^2 f_i^{(0)} \right] \\ & + \varepsilon^2 (q-1) \left[\delta(e_i \cdot \nabla_1) f_i^{(1)} + \frac{1}{2} \delta^2 (e_i \cdot \nabla_1)^2 f_i^{(0)} \right] = -\frac{\varepsilon^2}{\tau} f_i^{(2)} \end{aligned} \quad (\text{A9})$$

in the order of $O(\varepsilon^2)$. Equation (A9) can be reduced to

$$\begin{aligned} & \varepsilon^2 \left[\delta \partial_{t^1} f_i^{(0)} + \delta(\partial_{t^0} + q e_i \cdot \nabla_1) f_i^{(1)} + \frac{1}{2} \delta^2 [(\partial_{t^0} + e_i \cdot \nabla_1)^2 \right. \\ & \left. + (q-1)(e_i \cdot \nabla_1)^2] f_i^{(0)} \right] = -\frac{\varepsilon^2}{\tau} f_i^{(2)}. \end{aligned} \quad (\text{A10})$$

Substituting (A8) into (A10) gives

$$\begin{aligned} & \varepsilon^2 \left\{ \delta \partial_{t^1} + \delta^2 \left[\left(\frac{1}{2} - \tau \right) \partial_{t^0}^2 + \left(\frac{q}{2} - \tau q^2 \right) (e_i \cdot \nabla_1)^2 \right. \right. \\ & \left. \left. + (-2\tau q + 1) \partial_{t^0} e_i \cdot \nabla_1 \right] \right\} f_i^{(0)} = -\frac{\varepsilon^2}{\tau} f_i^{(2)}. \end{aligned} \quad (\text{A11})$$

By summation of Eqs. (A8) and (A11), we have

$$\begin{aligned} & \delta(\varepsilon \partial_{t^0} + \varepsilon q e_i \cdot \nabla_1 + \varepsilon^2 \partial_{t^1}) f_i^{(0)} + \delta^2 \varepsilon^2 \left[\left(\frac{1}{2} - \tau \right) \partial_{t^0}^2 \right. \\ & \left. + (-2\tau q + 1) \partial_{t^0} e_i \cdot \nabla_1 \right] f_i^{(0)} + \varepsilon^2 \left(\frac{q}{2} - \tau q^2 \right) (e_i \cdot \nabla_1)^2 f_i^{(0)} \\ & = -\frac{\varepsilon f_i^{(1)} + \varepsilon^2 f_i^{(2)}}{\tau}. \end{aligned} \quad (\text{A12})$$

Thus, to the order of $O(\varepsilon^2)$, we have

$$\begin{aligned} & \delta(\partial_t + q e_i \cdot \nabla) f_i^{(0)} + \delta^2 \left[\left(\frac{1}{2} - \tau \right) \partial_t^2 + (-2\tau q + 1) \partial_t e_i \cdot \nabla \right] f_i^{(0)} \\ & + \delta^2 \left(\frac{q}{2} - \tau q^2 \right) (e_i \cdot \nabla)^2 f_i^{(0)} + O(\delta^3) = \Omega_i. \end{aligned} \quad (\text{A13})$$

From Eq. (A13), we have

$$\partial_t \sum_i f_i^{(0)} + \nabla \cdot \left(q \sum_i f_i^{(0)} e_i \right) + O(\delta) = 0, \quad (\text{A14})$$

$$\begin{aligned} & \partial_t \sum_i f_i^{(0)} + \nabla \cdot \left(q \sum_i f_i^{(0)} e_i \right) + \delta \left[\left(\frac{1}{2} - \tau \right) \partial_t^2 \sum_i f_i^{(0)} \right. \\ & \left. + (-2\tau q + 1) \partial_t \nabla \cdot \sum_i f_i^{(0)} e_i \right] \\ & + \delta \left(\frac{q}{2} - \tau q^2 \right) \nabla \nabla : \sum_i f_i^{(0)} e_i e_i + O(\delta^2) = 0. \end{aligned} \quad (\text{A15})$$

The conservation laws give

$$\sum_i f_i^{(0)} = \phi, \quad (\text{A16})$$

$$\sum_i f_i^{(0)} e_{i\alpha} \equiv \frac{\phi}{q} u_\alpha, \quad (\text{A17})$$

$$\sum_i f_i^{(0)} e_{i\alpha} e_{i\beta} \equiv \Xi_{\alpha\beta}. \quad (\text{A18})$$

Thus, Eq. (A14) and Eq. (A15) can be reexpressed as

$$\partial_t \phi + \nabla \cdot (\phi u) + O(\delta) = 0, \quad (\text{A19})$$

$$\begin{aligned} & \partial_t \phi + \nabla \cdot (\phi u) + \delta \left[\left(\frac{1}{2} - \tau \right) (\partial_t^2 \phi + \partial_t \nabla \cdot (\phi u)) \right. \\ & \left. + \left(\frac{-2\tau q + 1}{q} + \tau - \frac{1}{2} \right) \partial_t \nabla \cdot (\phi u) \right] \\ & + \left(\frac{q}{2} - \tau q^2 \right) \delta \nabla \nabla : \Xi + O(\delta^2) = 0. \end{aligned} \quad (\text{A20})$$

As indicated [Eq. (B2)] in the appendix of Swift *et al.* [17], the first and second terms in the bracket of Eq. (A20) are of higher order and can be neglected. So, Eq. (A20) can be written as

$$\begin{aligned} & \partial_t \phi + \nabla \cdot (\phi u) + \left(\frac{q}{2} - \tau q^2 \right) \delta \nabla \nabla : \Xi \\ & + \left(\frac{-2\tau q + 1}{q} + \tau - \frac{1}{2} \right) \delta \partial_t \nabla \cdot (\phi u) + O(\delta^2) = 0. \end{aligned} \quad (\text{A21})$$

Thus, if we set,

$$\frac{-2\tau q + 1}{q} + \tau - \frac{1}{2} = 0, \quad (\text{A22})$$

that is,

$$q = \frac{1}{\tau + 0.5},$$

then the time derivative term will be removed.

Beside, the momentum flux term is set to

$$\Xi_{\alpha\beta} = \Gamma \mu \delta_{\alpha\beta}. \quad (\text{A23})$$

Thus we will recover the Cahn Hilliard equation to the second order without any additional terms:

$$\partial_t \phi + \nabla \cdot (\phi u) - q \left(\tau q - \frac{1}{2} \right) \Gamma \delta \nabla^2 \mu + O(\delta^2) = 0. \quad (\text{A24})$$

-
- [1] M. R. Swift, W. R. Osborn, and J. M. Yeomans, *Phys. Rev. Lett.* **75**, 830 (1995).
- [2] A. Lamura and G. Gonnella, *Physica A* **294**, 295 (2001).
- [3] A. Cristea and V. Sofonea, *Int. J. Mod. Phys. C* **14**, 1251 (2003).
- [4] T. Inamuro, T. Ogata, S. Tajima, and N. Konishi, *J. Comput. Phys.* **198**, 628 (2004).
- [5] I. Ginzburg and K. Steiner, *Philos. Trans. R. Soc. London, Ser. A* **360**, 453 (2002).
- [6] C. K. Aidun, E-Jiang Ding, and Y. Lu, *J. Fluid Mech.* **373**, 287 (1998).
- [7] C. W. Hirt and B. D. Nichols, *J. Comput. Phys.* **39**, 201 (1981).
- [8] M. Rudman, *Int. J. Numer. Methods Fluids* **24**, 671 (1997).
- [9] W. J. Rider and B. D. Kothe, *J. Comput. Phys.* **141**, 112 (1998).
- [10] O. Ubbink and R. I. Issa, *J. Comput. Phys.* **153**, 26 (1999).
- [11] J. E. Pilliod, Jr. and E. G. Puckett, *J. Comput. Phys.* **199**, 465 (2004).
- [12] S. Osher and J. A. Sethian, *J. Comput. Phys.* **79**, 12 (1988).
- [13] D. Kothe, D. Juric, S. J. Mosso, and B. Lally, *Modelling of Casting, Welding and Advanced Solidification Processes VIII*, edited by B. G. Thomas and C. Beckermann (TMS, San Diego, 1998), pp. 17–28.
- [14] D. H. Rothman and J. M. Keller, *J. Stat. Phys.* **52**, 1119 (1988).
- [15] A. K. Gunstensen, D. H. Rothman, S. Zaleski, and G. Zanetti, *Phys. Rev. A* **43**, 4320 (1991).
- [16] X. Shan and H. Chen, *Phys. Rev. E* **47**, 1815 (1993).
- [17] M. R. Swift, E. Orlandini, W. R. Osborn, and J. M. Yeomans, *Phys. Rev. E* **54**, 5041 (1996).
- [18] J. W. Cahn and J. E. Hilliard, *J. Chem. Phys.* **2**, 258 (1958).
- [19] M. Rudman, *Int. J. Numer. Methods Fluids* **28**, 357 (1998).
- [20] M. Sussman, E. Fatemi, P. Smereka, and S. Osher, *Comput. Fluids* **27**, 663 (1998).
- [21] J. S. Rowlinson and B. Widom, *Molecular Theory of Capillarity* (Clarendon, Oxford, 1989).
- [22] A. Lamura and S. Succi, *Int. J. Mod. Phys. B* **17**, 145 (2003).
- [23] P. Bhatnagar, E. P. Gross, and M. K. Krook, *Phys. Rev.* **94**, 511 (1954).
- [24] D. Jacqmin, *J. Comput. Phys.* **155**, 96 (1999).
- [25] M. Rudman, *Int. J. Numer. Methods Fluids* **24**, 671 (1997).